IEEE Access
Multidisciplinary | Rapid Review | Open Access Journal

Received August 27, 2019, accepted September 5, 2019, date of publication September 11, 2019,
date of current version September 23, 2019.

Digital Object Identifier 10.1109/ACCESS.2019.2940214

Designed Dynamic Reference With Model Predictive Control for Bidirectional EV Chargers

TINGTING HE[1], (Student Member, IEEE), MINGLI WU[1], DYLAN DAH-CHUAN LU[2], (Senior Member, IEEE), RICARDO P. AGUILERA[2], (Member, IEEE), JIANWEI ZHANG[3], AND JIANGUO ZHU[4], (Senior Member, IEEE)

[1]School of Electrical Engineering, Beijing Jiaotong University, Beijing 100044, China
[2]School of Electrical and Data Engineering, University of Technology Sydney, Sydney, NSW 2007, Australia
[3]College of Electric Power, Inner Mongolia University of Technology, Hohhot 010062, China
[4]School of Electrical and Information Engineering, The University of Sydney, Sydney, NSW 2006 Australia

Corresponding author: Mingli Wu (mlwu@bjtu.edu.cn)

This work was supported in part by the Fundamental Research Funds for the Central Universities under Grant 2018JBZ101.

ABSTRACT This paper presents a finite control set model predictive control (MPC) using a designed dynamic reference for bidirectional electric vehicle (EV) chargers. In the conventional MPC scheme, a PI controller is involved to generate an active power reference from the DC voltage reference. It is hard to find one fixed set of coefficients for all working conditions. In this paper, a designed dynamic reference based MPC strategy is proposed to replace the PI control loop. In the proposed method, a DC voltage dynamic reference is developed to formulate the inherent relationship between the DC voltage reference and the active power reference. Multi-objective control can be achieved in the proposed scheme, including controlling of the DC voltage, battery charging/discharging current, active power and reactive power, independently. Bidirectional power flow is operated effectively between the EV- and the grid-side. Experimental results are obtained from a laboratory three-phase two-stage bidirectional EV charger controlled by dSPACE DS1104. The results show that fast dynamic and good steady state performance of tracking the above objectives can be achieved with the proposed method. Compared with the system performance obtained by the conventional MPC method, the proposed method generates less active power ripples and produces a better grid current performance.

INDEX TERMS Model predictive control, dynamic reference, bidirectional charger, electric vehicle.

I. INTRODUCTION

Due to the clean and efficient features, electric vehicles (EVs) are expected to play an important role in transportation in the near future [1]. With the advanced battery technology and control schemes, EVs have been widely used in many applications, such as transportation [3], public service [4] and private vehicles [5]. Currently, EVs are starting to penetrate into the main power grid and distributed systems as a new major load [6]. Similar to the current electrical loads, EV batteries consume energy provided by the power system, which is known as the grid-to-vehicle (G2V) operation. On the other hand, EV batteries can be regarded as energy storage devices to supply active power to the grid, or so-called vehicle-to-grid (V2G) operation [7], [8].

The associate editor coordinating the review of this manuscript and approving it for publication was Sudhakar Babu Thanikanti.

As a critical component in electrified transportation, EV batteries support the main grid by charging or discharging the active power from or to the grid via on or off-board unidirectional or bidirectional chargers [9]. The unidirectional chargers only transmit the active power from the grid to the EV batteries at a unity power factor generally. In order to achieve a two-way delivery of the active power, bidirectional topologies have been studied [10], [11]. Apart from exchanging the active power between the EV batteries and the power grid, known as V2G and G2V operations, it is possible for the EV to produce or consume the reactive power in connection with the grid. This operation mode is known as the vehicle-for-grid (V4G) mode, where the EV batteries can be applied as the static VAR compensators to compensate the reactive power in the utility grid. To meet this demand, bidirectional EV charging stations need to be installed at residential and commercial locations.

This work is licensed under a Creative Commons Attribution 4.0 License. For more information, see http://creativecommons.org/licenses/by/4.0/

In [12], Kesler *et al*. proposed a V2G reactive power operation for a single-phase on-board EV charger, where the charger operates in G2V mode with or without exchanging the reactive power. The authors have also studied a three-phase off-board fast charger in [13] to work in the positive axis of active power in the PQ plane. As an example, in [14], EVs are studied to provide reactive power to the main grid and compensate current harmonics in smart homes with a single-phase charger. Compared with the single-phase chargers used in smart homes, a three-phase two-stage bidirectional battery charger is more suitable for commercial applications.

Different methods have been used for controlling EV chargers, such as the proportional integral (PI) control, the voltage-oriented control (VOC) and the direct power control (DPC) [15]–[18]. An external voltage loop and an inner current loop are used in the VOC scheme. The PI controllers are required in VOC to generate the reference values used in the associated space vector modulation. Derived from the direct toque control (DTC) for motor control, DPC is another popular control scheme for power converters, which can have fast dynamic performance. A designed switching table is used to select an optimal switching state [19]. Unlike the PI controller, the DPC does not need the phase-locked loop (PLL), the internal current loop or modulators. However, this method introduces high power ripples, which leads to highly distorted grid currents [20].

Recently, a finite control set model predictive control (MPC) have emerged on controlling the power electronics [21]–[23]. Compared with the pure PI control, VOC and DPC methods, no extra voltage/current loops, modulator or PLL are needed in MPC strategy. The main advantage of MPC is that the modulation and synchronization are not required and the system constrains can be added directly in the cost function [24]. Based on the system model, a switching state is selected to minimize the cost function which is designed as a function of the errors of the controlled variables [25], [26].

With the MPC method, the active and reactive power can be tracked effectively. Since the DC-link voltage and active power are coupled, a PI controller is applied in the conventional MPC method to obtain the grid active power reference from the DC-link voltage reference [27]. Then, the generated active power reference and given reactive power reference are transferred to the cost function to choose an optimal switching state for the next sampling time. However, due to the discrete-time switching nature of the converter, it is always a difficult task to tune the PI coefficients by trial-and-error method. When the system operation condition changes, the selected P and I coefficients may not suit the new requirements for the updated system parameters. To solve this problem, some methods, such as adaptive PI control and adaptive reference voltage, were proposed and studied [28], [29]. The outer loop voltage regulator and the inner loop current regulator were still used in the proposed adaptive PI controller. Four dynamic control gains were regulated to maintain the error within the accepted value via several control loops. With the proposed method in [29], system performance can be improved compared to the results from the conventional PI controller. However, the system performance depends on the designed error. If a small error is applied, better performance can be achieved at the expense of longer calculation time for the loop of the adaptive-tuning PI controller. To avoid the problem introduced by the cascaded control loop, such as PI controller, a dynamic active power reference obtained from a filtered DC voltage reference is designed in this study. For a two-stage EV charger, the active power reference is also associated with the load current. Therefore, the proposed method formulates the inherent relationship among the active power, DC voltage and battery current references. Charging and discharging operations are discussed in detail separately.

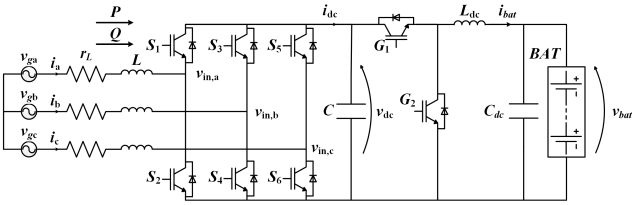

FIGURE 1. Circuit topology of AC/DC converter connected with battery via a DC/DC converter.

The rest of this paper is organized as follows. In Section II, a system model for the bidirectional EV charger is presented. The MPC scheme principle for this two-stage charger is also detailed in this section. Section III shows the design of the proposed dynamic reference during the charging and discharging operations. Simulation and experimental results are presented in Section IV. Finally, the conclusions are drawn in Section V.

II. MPC OF BIDIRECTIONAL EV CHARGERS

Since the chargers are designed for dynamic and different charging and discharging demands, a DC/DC bidirectional converter is used as the second stage to track the battery voltage [30]. The use of a second-stage DC/DC converter makes it suitable for different EV battery voltages [31], [32]. The DC/DC converter operates as a buck type converter when the battery is charged from the main grid. On the other hand, it is controlled as a boost-type converter for V2G operation. Therefore, the off-board bidirectional charger prototype used in this research project is composed of a 2-level three-phase AC/DC converter and a DC/DC converter, as shown in Fig. 1. The first stage, an AC/DC front end converter, is connected to the three-phase grid voltage via a filter inductor (L) and a resistance (r_L) connected in series. A filter capacitor (C) is connected on the DC-side to filter the DC voltage (v_{dc}). For the second stage, the DC/DC rear-end converter consists of two insulated-gate bipolar transistor-diode switches (G_1 and G_2). The DC/DC converter is used to interface with the EV battery through an output inductor (L_{dc}). A filter capacitor (C_{dc}) is connected in parallel with the EV battery.

The switching state of the three-phase AC/DC converter can be determined by gating signals S_a, S_b and S_c on each phase, which are defined as

$$S_k = \begin{cases} 1 & \text{upper switch on phase } k \text{ is on} \\ 0 & \text{lower switch on phase } k \text{ is on,} \end{cases} \quad (1)$$

where $k = a, b, c$. For example, $S_a = 1$ means, on the A-phase, S_1 is on and S_2 is off.

According to the space vector pulse width modulation (SVPWM), eight possible switching states can be generated in a stationary two-axis reference frame (the $\alpha\beta$ coordinate system) as:

$$\mathbf{S}_{\alpha\beta} = \frac{2}{3}\begin{bmatrix} 1 & -\frac{1}{2} & -\frac{1}{2} \\ 0 & \frac{\sqrt{3}}{2} & -\frac{\sqrt{3}}{2} \end{bmatrix} \mathbf{S_{abc}}, \quad (2)$$

where

$$\mathbf{S}_{\alpha\beta} = \begin{bmatrix} S_\alpha \\ S_\beta \end{bmatrix}, \quad \mathbf{S_{abc}} = \begin{bmatrix} S_a \\ S_b \\ S_c \end{bmatrix}.$$

Then the input voltage (v_{in}) of the three-phase AC/DC converter in the $\alpha\beta$ coordinate can be expressed by using the switching matrix as:

$$\mathbf{v}_{\alpha\beta} = \begin{bmatrix} v_\alpha \\ v_\beta \end{bmatrix} = \mathbf{S}_{\alpha\beta} v_{dc} = \begin{bmatrix} S_\alpha \\ S_\beta \end{bmatrix} v_{dc}. \quad (3)$$

These eight input voltage vectors of the converter can be obtained from the eight possible switching states, as listed in Table 1.

It is assumed that a balanced three-phase grid power supply is provided in the system (in Fig. 1). Applying Kirchoff's voltage law and the standard $\alpha\beta$ frame transformation, one can express the input current dynamic of the charger's first-stage in the vector form as

$$L\frac{d\mathbf{i}_{\mathbf{g},\alpha\beta}}{dt} = \mathbf{v}_{\mathbf{g},\alpha\beta} - r_L\mathbf{i}_{\mathbf{g},\alpha\beta} - \mathbf{v}_{\alpha\beta}, \quad (4)$$

where $\mathbf{v}_{\mathbf{g},\alpha\beta}$ and $\mathbf{i}_{\mathbf{g},\alpha\beta}$ are the grid input voltage and current vectors in the $\alpha\beta$ frame, respectively, calculated by

$$\mathbf{v}_{\mathbf{g},\alpha\beta} = \begin{bmatrix} v_{g,\alpha} \\ v_{g,\beta} \end{bmatrix} = \frac{2}{3}\begin{bmatrix} 1 & -\frac{1}{2} & -\frac{1}{2} \\ 0 & \frac{\sqrt{3}}{2} & -\frac{\sqrt{3}}{2} \end{bmatrix} \begin{bmatrix} v_{g,a} \\ v_{g,b} \\ v_{g,c} \end{bmatrix},$$

$$\mathbf{i}_{\mathbf{g},\alpha\beta} = \begin{bmatrix} i_{g,\alpha} \\ i_{g,\beta} \end{bmatrix} = \frac{2}{3}\begin{bmatrix} 1 & -\frac{1}{2} & -\frac{1}{2} \\ 0 & \frac{\sqrt{3}}{2} & -\frac{\sqrt{3}}{2} \end{bmatrix} \begin{bmatrix} i_{g,a} \\ i_{g,b} \\ i_{g,c} \end{bmatrix}.$$

Based on the forward Euler approximation, the derivative of the input currents in the continuous-time model can be represented with a sampling period T_s as

$$\frac{d\mathbf{i}_{\mathbf{g},\alpha\beta}}{dt} = \frac{\mathbf{i}_\mathbf{g}(k+1) - \mathbf{i}_\mathbf{g}(k)}{T_s}. \quad (5)$$

TABLE 1. The converter voltage vectors in $\alpha\beta$ coordinate.

NO.	S_a	S_b	S_c	S_α	S_β	v_α	v_β	$\|v_\alpha+jv_\beta\|$
0	0	0	0	0	0	0	0	0
1	1	0	0	$\frac{2}{3}$	0	$\frac{2v_{dc}}{3}$	0	$\frac{2v_{dc}}{3}$
2	1	1	0	$\frac{1}{3}$	$\frac{1}{\sqrt{3}}$	$\frac{v_{dc}}{3}$	$\frac{v_{dc}}{\sqrt{3}}$	$\frac{2v_{dc}}{3}$
3	0	1	0	$-\frac{1}{3}$	$\frac{1}{\sqrt{3}}$	$-\frac{v_{dc}}{3}$	$\frac{v_{dc}}{\sqrt{3}}$	$\frac{2v_{dc}}{3}$
4	0	1	1	$-\frac{2}{3}$	0	$-\frac{2v_{dc}}{3}$	0	$\frac{2v_{dc}}{3}$
5	0	0	1	$-\frac{1}{3}$	$-\frac{1}{\sqrt{3}}$	$-\frac{v_{dc}}{3}$	$-\frac{v_{dc}}{\sqrt{3}}$	$\frac{2v_{dc}}{3}$
6	1	0	1	$\frac{1}{3}$	$-\frac{1}{\sqrt{3}}$	$\frac{v_{dc}}{3}$	$-\frac{v_{dc}}{\sqrt{3}}$	$\frac{2v_{dc}}{3}$
7	1	1	1	0	0	0	0	0

The grid current (4) can be expressed in the discrete-time domain as

$$\mathbf{i}_\mathbf{g}(k+1) = \frac{T_s}{L}(\mathbf{v}_{\mathbf{g},\alpha\beta}(k) - R\mathbf{i}_{\mathbf{g},\alpha\beta}(k) - \mathbf{v}_{\alpha\beta}(k)) + \mathbf{i}_{\mathbf{g},\alpha\beta}(k) \quad (6)$$

Eight possible values of instantaneous power transmitting from the grid to the battery at the $(k+1)$th instant can be predicted on the basis of the eight predicted input currents as

$$\begin{aligned} P_g(k+1) &= \frac{3}{2}Re\left\{\mathbf{v_g}\mathbf{i}_\mathbf{g}^*\right\} \\ &= \frac{3}{2}(v_{g,\alpha}(k+1)i_{g,\alpha}(k+1) + v_{g,\beta}(k+1)i_{g,\beta}(k+1)) \end{aligned} \quad (7)$$

$$\begin{aligned} Q_g(k+1) &= \frac{3}{2}Im\left\{\mathbf{v_g}\mathbf{i}_\mathbf{g}^*\right\} \\ &= \frac{3}{2}(v_{g,\beta}(k+1)i_{g,\alpha}(k+1) - v_{g,\alpha}(k+1)i_{g,\beta}(k+1)) \end{aligned} \quad (8)$$

where $v_{g,\alpha}(k+1)$, $v_{g,\beta}(k+1)$, $i_{g,\alpha}(k+1)$ and $i_{g,\beta}(k+1)$ are the predicted grid voltage and current values at the $(k+1)$th instant in the $\alpha\beta$ coordinate.

To avoid short circuit, the switches G_1 and G_2 in the second stage are operated in a complementary manner. Therefore, the switching state G can be defined as: when G_1 is on and G_2 is off, the switching state G is equal 1. Otherwise, G is defined as 0.

The mathematical model of the DC/DC bidirectional converter can be expressed as

$$G(k)v_{dc}(k) = L\frac{di_{bat}(k)}{dt} + v_{bat}(k). \quad (9)$$

where v_{dc} is the DC capacitor voltage, v_{bat} and i_{bat} are, respectively, the instantaneous values of voltage and current of the EV battery.

Then, the battery current can be calculated in the discrete time domain as

$$i_{bat}(k+1) = i_{bat}(k) + \frac{T_s}{L}(G(k)v_{dc}(k) - v_{bat}(k)). \quad (10)$$

The main objective of the first-stage AC/DC converter is to deliver the active power P_g from the grid to the EV battery or in an opposite direction. Generally, the average active power $P_g(t)$ provided by the grid is equal to the sum of the average power delivered by the AC/DC converter $P_{load}(t)$ and

the power loss in the inductor resistance $P_{loss}(t)$. If we ignore the power loss, the power provided by the grid is the same as the power transferred by the converter, $P_{load}(t) = P_g(t)$. However, the instantaneous grid active power $P_g(t)$ cannot be calculated by the above relationship. For example, when the voltage vector is chosen as the NO.1 or 8 in Table 1, $S_a = S_b = S_c$, there is no power delivered from the AC/DC converter, $P_{load}(t) = 0$, while the grid power $P_g(t) \neq 0$. In the previous work, many researchers used a PI controller to present the inherent relationship between the DC-link voltage and the active power [21], [25]. An active power reference P_g^{ref} is generated from the DC voltage reference v_{dc}^{ref} via a PI controller. Since the PI coefficients are hard to be tuned for the best performance, a filtered DC voltage reference $\widetilde{v}_{dc}^{ref}$ is introduced to develop the inherent relationship, as detailed in the Section III.

Besides the active power, the reactive power is another target for the AC/DC converter. The EV charger can function as a static VAR compensator by regulating the reactive power. For the DC/DC converter, the objective is to track the battery current reference to charge or discharge the EV battery. Therefore, there are four targets for this MPC scheme, including the DC-link voltage v_{dc}, the grid active power P_g, the grid reactive power Q_g and the battery current i_{bat}. To achieve this multi-objective control, a cost function J is designed to select the switching state $\mathbf{S}(k)$ and $\mathbf{G}(k)$ that can minimize this cost function as

$$\left.\begin{aligned} J(k) = {} & \tfrac{1}{v_{dc}^{rated}}(\widetilde{v}_{dc}^{ref}(k+1) - v_{dc}(k+1))^2 \\ & + \tfrac{k_p}{P_g^{rated}}(P_g^{ref}(k+1) - P_g(k+1))^2 \\ & + \tfrac{k_q}{Q_g^{rated}}(Q_g^{ref}(k+1) - Q_g(k+1))^2 \end{aligned}\right\} = J_1$$
$$\left. + \tfrac{k_i}{i_{bat}^{rated}}(i_{bat}^{ref}(k+1) - i_{bat}(k+1))^2. \right\} = J_2 \quad (11)$$

where k_p, k_q and k_i are the weighing factors for the active power, reactive power and battery current, and the superscript ^{rated} and ^{ref} refer to the rated and reference values. In this work, all the objectives are equally important and hence sharing same weight. Therefore, in the simulation and experiment, k_p, k_q and k_i are designed to 1 in the proposed controller. The rated values v_{dc}^{rated}, P_g^{rated}, Q_g^{rated} and i_{bat}^{rated} are selected as 200 V, 300 W, 200 VAR and 2 A, respectively. J_1 and J_2 are the cost functions for AC/DC and DC/DC converters, respectively, as shown in (11). Firstly, a switching state $G(k)$ for the DC/DC converter is chosen to minimize the latter cost function J_2. Then, one optimal switching state $S(k)$ for the first stage AC/DC converter is selected to minimize the cost function J_1.

III. DYNAMIC REFERENCE DESIGN

As discussed in the Introduction, a main issue of the two-stage bidirectional charger is that the system cannot track the power, DC-link voltage and battery current effectively for arbitrarily chosen and time-varying reference demands. The active power $P_g(k)$, DC-link voltage $v_{dc}(k)$ and battery current $i_{bat}(k)$ are inescapably pair-wise coupled. It is difficult

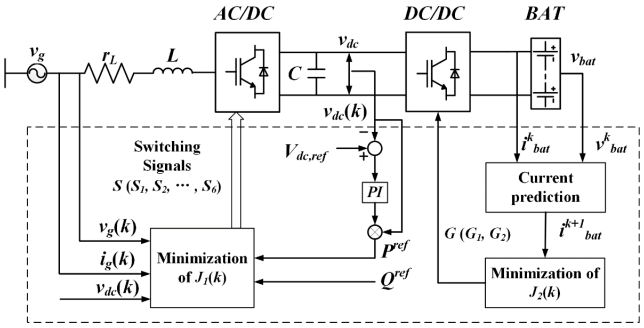

FIGURE 2. Control block of the conventional MPC method.

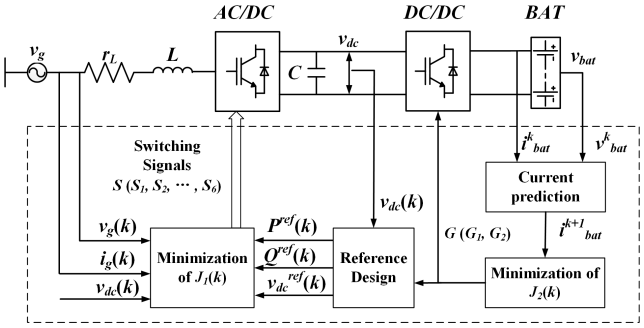

FIGURE 3. MPC with dynamic reference design for EV charger.

to find an exact closed form to describe their relationships because they depend on not only the sytem electrical parameters, but also on the applied switching law [33]. A conventional way to solve this problem is to use an additional PI control loop, where the active power reference is generated from the DC voltage via a PI controller [27], as shown in Fig. 2. With the designed PI controller, the system can work effectively to track the reference in the steady state. However, the proportional and integral factors are difficult to tune. When the reference signal or loads vary, a new set of PI parameters are required to update or tune to follow the new system demands, mainly because of the discrete-time switching system for the converters.

In this section, an alternative method is proposed to find the relationship between the active power $P_g(k)$, DC-link voltage $v_{dc}(k)$ and battery current $i_{bat}(k)$. The grid power reference is achieved directly from the MPC method via the filtered DC-voltage reference $\widetilde{v}_{dc}^{ref}$ and the given battery current reference signals i_{bat}^{ref}. No extra control loop or controller is required. To protect the system components and avoid integrator windup problem, the constraints for the maximum power level are designed in this section.

With the provided references $i_{bat}^{ref}(k)$, $v_{dc}^{ref}(k)$ and $Q^{ref}(k)$ and the measured system states $v_g(k)$, $i_g(k)$ and $v_{dc}(k)$, the dynamic reference design problem is to find the compatible reference for $P_g^{ref}(k)$ and the filtered reference $\widetilde{v}_{dc}^{ref}(k)$ used in the cost function J_1, as shown in Fig. 3. We first note that the capacitor or DC-link voltage $v_{dc}(k)$ is only determined by the capacitor current i_c. Another point is that the compatible reference for $P_g^{ref}(k)$ is associated with the filtered

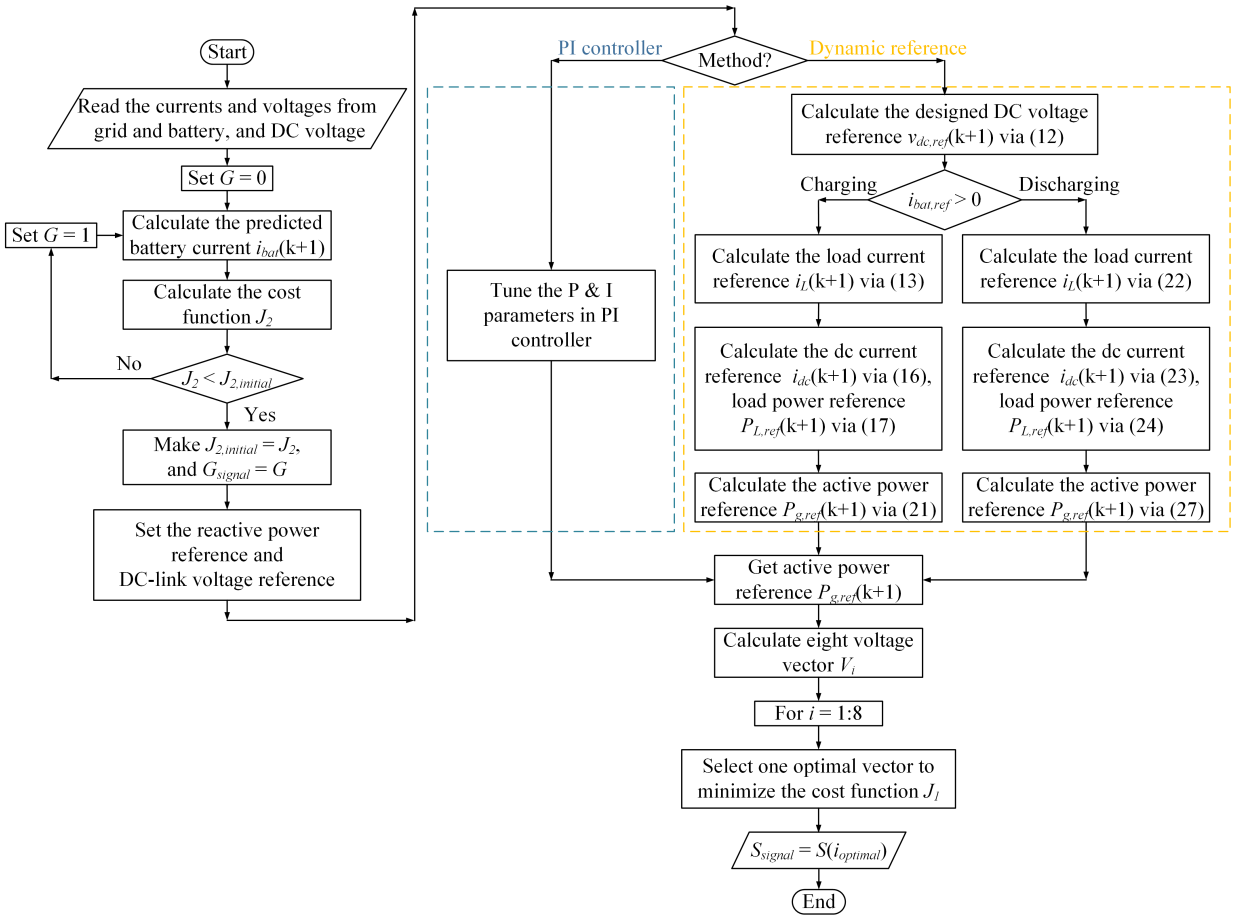

FIGURE 4. Flowchart of the proposed MPC method and the conventional algorithm.

reference $\tilde{v}_{dc}^{ref}(k)$, the battery current reference $i_{bat}^{ref}(k)$ and the switching signals for the second stage of the bidirectional EV charger. These switching states are obtained from the previous MPC method with the cost function J_2 in Section II. The reference $P_g^{ref}(k)$ formulas for the charging and discharging modes are different, since the current direction changes in different operations. The flowchart of the proposed method and the conventional MPC scheme is shown in Fig. 4.

To get the filtered reference signal $\tilde{v}_{dc}^{ref}$, a reference prediction horizon M is introduced. Then, the filtered reference signal $\tilde{v}_{dc}^{ref}$ is obtained from

$$\tilde{v}_{dc}^{ref}(k+1) = v_{dc}(k) + \frac{1}{M}(v_{dc}^{ref}(k) - v_{dc}(k)), \tag{12}$$

where the system performance is influenced by the reference prediction horizon M. If M is designed as a small value, the filtered reference $\tilde{v}_{dc}^{ref}$ is large, which leads to a faster tracking response. However, from the capacitor V-I characteristic, a large voltage variation increases the capacitor current. Therefore, to incorporate the current limitation and good dynamic response, a suitable value of M is selected in the simulation and experimental tests, as presented in Section IV.

A. DYNAMIC REFERENCE FOR CHARGING OPERATION

The actual current directions for the EV charger during the charging operation is presented in Fig. 5(a). The load current reference $i_L^{ref}(k+1)$ can be determined by the battery current reference as

$$i_L^{ref}(k+1) = G(k+1)i_{bat}^{ref}(k+1), \tag{13}$$

where $G(k+1)$ is the switching state for the second stage of the EV charger. It can be obtained from the MPC cost function J_1 to track the battery current reference.

It is important to note that the capacitor current reference $i_c^{ref}(k+1)$ is only controlled by the DC-link filtered voltage reference $\tilde{v}_{dc}^{ref}(k+1)$, and can be calculated by

$$i_c^{ref}(k+1) = C\frac{d(v_{dc}(k+1))}{T_s} = \frac{C}{T_s}(\tilde{v}_{dc}^{ref}(k+1) - v_{dc}(k)), \tag{14}$$

Substituting (12) into (14), one obtains:

$$i_c^{ref}(k+1) = \frac{C}{MT_s}(v_{dc}^{ref}(k) - v_{dc}(k)). \tag{15}$$

Therefore, the expected DC-link current i_{dc}^{ref} can be calculated as

$$i_{dc}^{ref}(k+1) = G(k+1)i_{bat}^{ref}(k+1) + \frac{C}{MT_s}(v_{dc}^{ref}(k) - v_{dc}(k)). \quad (16)$$

The transferred power which is required to track the filtered voltage $\tilde{v}_{dc}^{ref}(k+1)$ should satisfy

$$\begin{aligned} P_L^{ref}(k+1) &= i_{dc}^{ref}(k+1)\tilde{v}_{dc}^{ref}(k+1) \\ &= G(k+1)i_{bat}^{ref}(k+1)\tilde{v}_{dc}^{ref}(k+1) \\ &\quad + \frac{C}{MT_s}\tilde{v}_{dc}^{ref}(k+1)v_{dc}^{ref}(k) \\ &\quad - \frac{C}{MT_s}\tilde{v}_{dc}^{ref}(k+1)v_{dc}(k). \end{aligned} \quad (17)$$

During the charging operation, the load power $P_L^{ref}(k+1)$ is delivered from the AC-source to the EV battery. The power loss $P_{loss}^{ref}(k+1)$, which occurs in the AC inductor resistance r_L, can be obtained from the input power reference $P_g^{ref}(k+1)$, as

$$P_{loss}^{ref}(k+1) = \frac{2r_L}{3|V_s|^2}(P_g^{ref}(k+1)^2 + Q_g^{ref}(k+1)^2), \quad (18)$$

where $|V_s|$ is the amplitude of the grid voltage. On the other hand, the associated input active power reference $P_g^{ref}(k+1)$ transferred from the grid to the load can be calculated by

$$P_g^{ref}(k+1) = P_{loss}^{ref}(k+1) + P_L^{ref}(k+1). \quad (19)$$

It should be noted that the power loss P_{loss} is zero when the resistance r_L is equal to zero, which leads to its reference P_{loss}^{ref} equal to zero. Then, the active power reference P_g^{ref} can be calculated directly via P_L^{ref} using (19) during charging and discharging operations. When the resistance r_L can not be ignored, the active power reference P_g^{ref} can be deduced by the following steps.

Substituting (18) into (19), one obtains a quadratic equation with the source active power reference $P_g^{ref}(k+1)$ as the following

$$\frac{2r_L}{3|V_s|^2}P_g^{ref}(k+1)^2 - P_g^{ref}(k+1) + P_L^{ref}(k+1) + \frac{2r_L}{3|V_s|^2}Q_g^{ref}(k+1)^2 = 0. \quad (20)$$

Solving (20), the expected active power reference of $P_g^{ref}(k+1)$ can be deduced by

$$P_g^{ref}(k+1) = \frac{3|V_s|^2}{4r_L}\left(1 - \sqrt{1 - \frac{8r_L}{3|V_s|^2}a}\right). \quad (21)$$

where

$$a = P_L^{ref}(k+1) + \frac{2r_L}{3|V_s|^2}Q_g^{ref}(k+1)^2,$$

$P_L^{ref}(k+1)$ is obtained from (17) with the measured system state $v_{dc}(k)$, the given battery voltage reference $v_{dc}^{ref}(k)$, the given battery current reference $i_{bat}^{ref}(k+1)$ and the designed filtered reference $\tilde{v}_{dc}^{ref}(k+1)$.

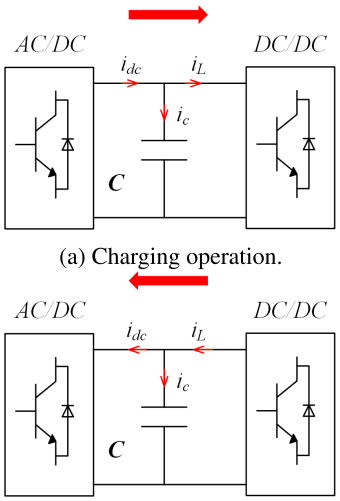

(a) Charging operation.

(b) Discharging operation.

FIGURE 5. Current direction in charging/discharging operation. (a) Charging operation. (b) Discharging operation.

B. DYNAMIC REFERENCE FOR DISCHARGING OPERATION

Fig. 5(b) shows the current flow during the discharging operation, from the load-side to the source-side. The direction of the load current reference $i_L^{ref}(k+1)$ is opposite from the battery reference. Therefore, the required load current reference $i_L^{ref}(k+1)$ can be expressed as

$$i_L^{ref}(k+1) = -G(k+1)i_{bat}^{ref}(k+1). \quad (22)$$

As mentioned, capacitor current i_c^{ref} in (15) can be used to find reference P_g^{ref}. Since the power changes its direction during the discharging operation, it requires a converter current reference $i_{dc}^{ref}(k+1)$ given by

$$i_{dc}^{ref}(k+1) = i_L^{ref}(k+1) - i_c^{ref}(k+1) \quad (23)$$

The AC/DC converter power reference $P_L^{ref}(k+1)$ can be expressed as

$$\begin{aligned} P_L^{ref}(k+1) &= i_{dc}^{ref}(k+1)\tilde{v}_{dc}^{ref}(k+1) \\ &= -G(k+1)i_{bat}^{ref}(k+1)\tilde{v}_{dc}^{ref}(k+1) \\ &\quad - \frac{C}{MT_s}\tilde{v}_{dc}^{ref}(k+1)v_{dc}^{ref}(k) \\ &\quad + \frac{C}{MT_s}\tilde{v}_{dc}^{ref}(k+1)v_{dc}(k). \end{aligned} \quad (24)$$

The power loss absorbed by the inductor resistances can also be calculated by using (18). In the discharging operation, the EV battery is regarded as a power source. Thus, the absorbed active power reference on the grid side $P_{g,a}^{ref}(k+1)$ can be expressed as

$$P_{g,a}^{ref}(k+1) = P_L^{ref}(k+1) - P_{loss}^{ref}(k+1), \quad (25)$$

where the actual direction for the absorbed power $P_{g,a}^{ref}(k+1)$ is delivering power from the EV battery to the grid side.

Substituting (18) into (25) when the resistance r_L is not zero, one can express the quadratic equation with the grid power $P^{ref}_{g,a}(k+1)$ as

$$\frac{2r_L}{3|V_s|^2}P^{ref}_{g,a}(k+1)^2 + P^{ref}_{g,a}(k+1) - P^{ref}_{L}(k+1) + \frac{2r_L}{3|V_s|^2}Q^{ref}_{g}(k+1)^2 = 0. \quad (26)$$

The solution to (26) shows the desired reference for $P^{ref}_{g,a}(k+1)$. To keep the same direction in the cost function, a negative sign should be added in front of $P^{ref}_{g,a}(k+1)$, and the designed active power reference $P^{ref}_{g}(k+1)$ in the discharging mode can be written as

$$P^{ref}_{g}(k+1) = -P^{ref}_{g,a}(k+1) = -\frac{3|V_s|^2}{4r_L}\left(-1+\sqrt{1+\frac{8r_L}{3|V_s|^2}b}\right), \quad (27)$$

where

$$b = P^{ref}_{L}(k+1) - \frac{2r_L}{3|V_s|^2}Q^{ref}_{g}(k+1)^2,$$

the actual direction for $P^{ref}_{g}(k+1)$ is from the grid-side to the load-side.

To protect the system components, a limitation for the active power is developed, which is associated with the maximum grid current [33], expressed as

$$|P^{ref}_{g}(k+1)| \le P^{max}_{g}(k+1), \le \sqrt{(1.5|Vs||I_{max}|)^2 - (Q^{ref}_{g}(k+1))^2}, \quad (28)$$

where I_{max} is the maximum current for the components.

IV. SIMULATION RESULTS

Some representative simulation results are presented in this section to demonstrate the performance of the proposed and conventional controllers. A three-phase converter in Fig. 1 is used as the EV charger in Matlab/Simulink, with the electrical parameters equal to $r_L = 0.025\ \Omega$, $L = 12$ mH, $L_{dc} = 35$ mH, and $C = 680\ \mu$F. The sampling frequency is set to be 40 kHz. The grid peak voltage is 50 V and the battery rated voltage is 144 V. The reference prediction horizon is set as M = 50. To perform a unity power factor operation, the reactive power reference is set to be 0 VAR. The battery charging current reference is 2 A.

The start-up and DC-link dynamic performance obtained from the conventional and proposed MPC schemes are provided in Fig. 6. The DC-link voltage reference is set to 200 V during the first half second. It can be seen that both two methods can track the DC voltage reference effectively. For the conventional MPC method, the proportional and integral parameters are fine tuned to achieve the best performance, equal to 0.1 and 1 in the simulation test, respectively. It takes around 0.2 s for the conventional method to reach the reference value without any state-state error. However, there is a small undershoot around 9 V during the start-up performance, as shown in Fig. 6(a). With the proposed method, the undershoot can be eliminated effectively, and the response time for can be reduced to 0.018 s. The response speed is around 10 times faster than the conventional one.

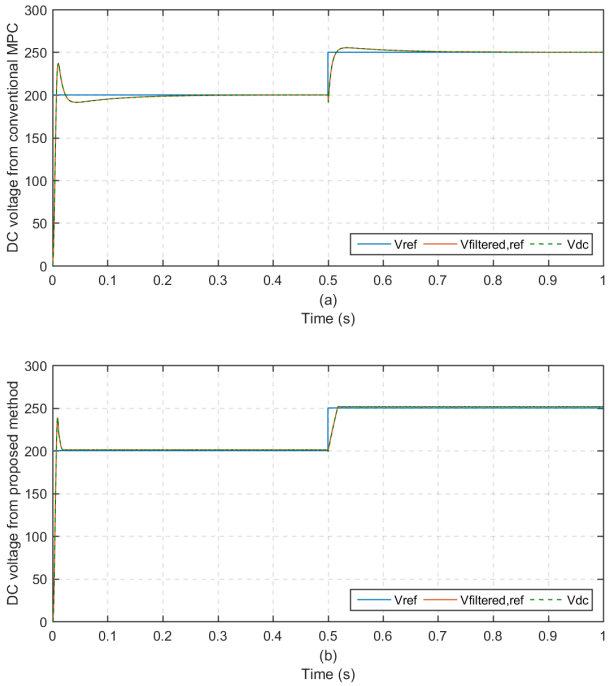

FIGURE 6. Start-up and dynamic performance.

Then, a voltage step is applied in the DC link voltage reference at time instant $t = 0.5$ s changing from 200 V to 250 V. Fig. 6 shows that the traditional method takes around 0.2 s to reach the new working condition. Compared with the conventional method with a overshoot 5 V on the DC voltage, the proposed method can reach the new voltage reference within 0.019 s without any overshoot.

Figs. 7 and 8 show the dynamic performance when a significant drop is applied in the battery current reference from 2 A to −2 A, changing from charging to discharging operation. The DC-link voltage is controlled to 200 V. For the conventional method with the PI controller, it takes around 0.3 s to recover to the original v_{dc} reference with a small overshoot equal to 23 V (approximately 11% of the steady-state value). With the proposed dynamic reference, there is no obvious change on the DC-link voltage when its reference keeps stable at 200 V. The active power obtained from the proposed method can track the new reference much faster than the traditional scheme.

When environment temperature or inaccurate measurements lead to an inaccurate system model, the proposed controller can still achieve acceptable performance, which means it depends on system model parameters slightly.

V. EXPERIMENTAL RESULTS

To verify the performance of the proposed predictive method for a bidirectional EV charger, numerous experimental tests

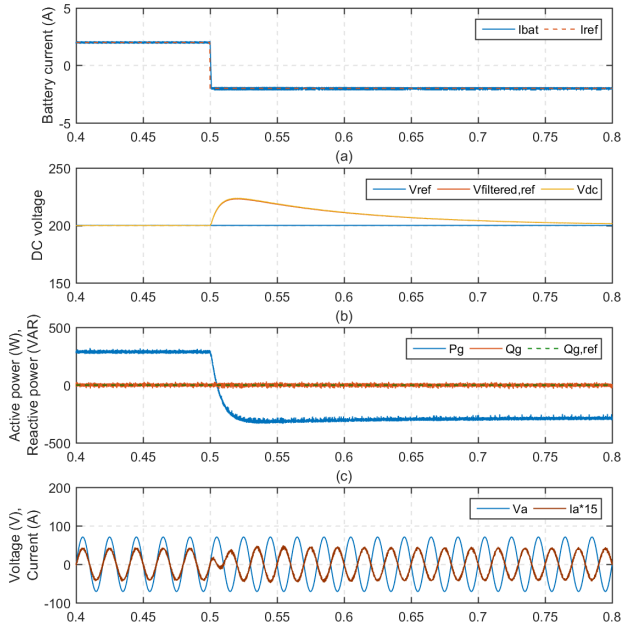

FIGURE 7. Simulation results from MPC during current changing operation.

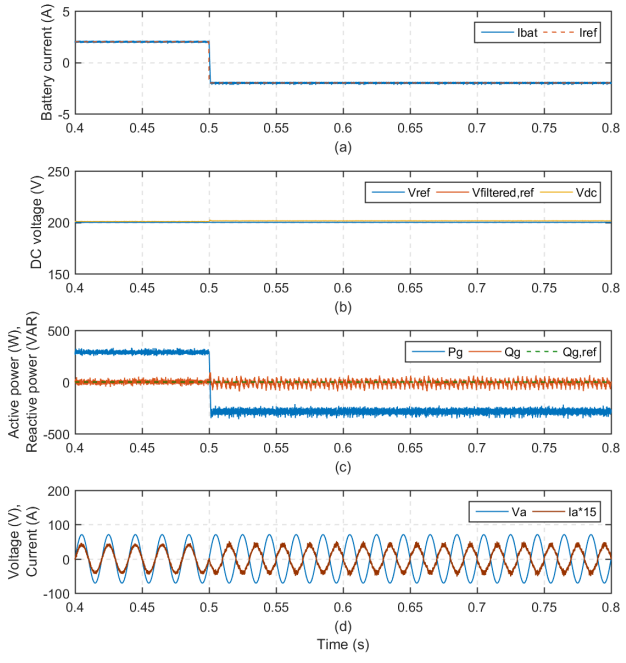

FIGURE 8. Simulation results from proposed method during current changing operation.

are carried out. Compared experimental tests of the conventional and proposed MPC methods are performed using a laboratory prototype of a three-phase two-stage EV charger, as shown in Fig. 9. The electrical parameters of the system are given by $r_L = 0.025\ \Omega$, $L = 8.8$ mH, $L_{dc} = 35$ mH, and $C = 680\ \mu$F. A lead-acid battery is used to emulate the EV battery with the nominal voltage $v_{bat} = 144$ V. The amplitude of grid voltage is chosen to be $|V_s| = 71$ V with

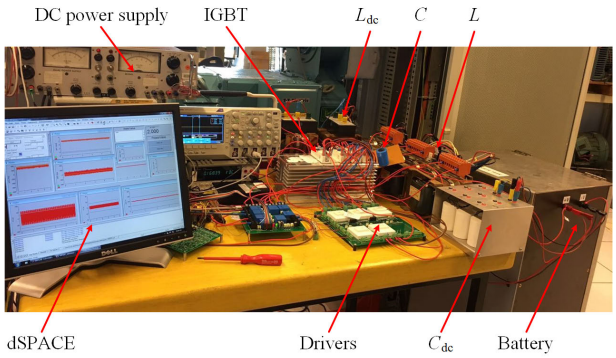

FIGURE 9. Experimental setup.

the grid frequency equal to 50 Hz. This voltage is obtained from a three-phase transformer connected with a 220 V rms grid. The sampling frequency f_s is 15 kHz, or the sampling period $T_s = 67\ \mu$s. The reference prediction horizon is set as $M = 50$. The experimental test is performed on a real-time interface system dSPACE with a DS1104 control desk.

A. PI PARAMETERS SELECTION

To achieve fair comparison, a standard rule to design the parameters of the PI controller for the conventional MPC is used [34].

Since the objective is to control the DC-link voltage, a parameter z is introduced to analysis the system plant, designed as

$$z = \frac{v_{dc}^2}{2}. \tag{29}$$

The first-order derivation of the designed parameter z can be calculated as

$$\dot{z} = v_{dc}\dot{v_{dc}}. \tag{30}$$

Then, the active power reference P_{ref} can be written as

$$\begin{aligned} P_{ref} &= Cv_{dc}\frac{v_{dc}}{dt} + v_{bat}i_{bat}^{ref} \\ &= Cz + v_{bat}i_{bat}^{ref}. \end{aligned} \tag{31}$$

The system plant can be expressed as

$$\begin{aligned} G(s) = \frac{z}{P_{ref}} &= \frac{z}{C\dot{z} + v_{bat}i_{bat}^{ref}} \\ &= \frac{1}{Cs + \frac{2v_{bat}i_{bat}^{ref}}{v_{dc}^2}} \\ &= \frac{K_o}{T_a s + 1}, \end{aligned} \tag{32}$$

where

$$K_o = \frac{v_{dc}^2}{2v_{bat}i_{bat}^{ref}}, \quad T_a = C\frac{v_{dc}^2}{2v_{bat}i_{bat}^{ref}} = CK_o.$$

According to the standard rules in Table 4.5 in Ref. [34], a damping factor selection method can be used in this kind of

system plant. The rate of the PI controller proportional and integral parameters, denoted as k_p/k_i can be designed as

$$\frac{k_p}{k_i} = \frac{4\xi^2 T_a K_o}{(1+K_o)^2} = \frac{4\xi^2 C K_o^2}{(1+K_o)^2} \tag{33}$$

where ξ is the damping ratio of the system, and recommended to be set as 0.707. Substituting the DC-link capacitor (680 uF), the battery rated voltage (144 V), the battery current reference (2 A) and the DC-link voltage reference (200 V) into (33), the rate as k_p/k_i is equal to 0.0013. Therefore, the parameters k_p/k_i are tuned based on this recommended rate. On the other hand, considering the overshoot and response speed, the proportional and integral parameters k_p and k_i, equal to 0.15 and 100, respectively, are selected to achieve the best performance of the conventional MPC method in the experimental test.

B. TRACKING OF BATTERY CURRENT AND ACTIVE POWER REFERENCE

Figs. 10 and 11 show the experimental results of battery current and active power reference tracking obtained from the traditional and proposed schemes, respectively. The DC voltage reference is set as $v_{dc}^{ref} = 200$ V. A unity power factor operation is designed, which leads to a null reactive power, that is, $Q_s^{ref} = 0$ VAR. At time instant $t = 0.52$ s in conventional MPC and 0.44 s in the proposed method, a decrease step is applied on the battery current reference i_{bat}^{ref} from 2 A to -2 A. The EV battery is controlled to operate from charging mode to discharging mode. Therefore, the desired source power follows the reference declining from around 300 W to -300 W. It can be noticed that both two control methods show a similar system behaviour. The conventional MPC and the proposed MPC with dynamic reference method can track the current reference effectively, as depicted in Figs. 10(a) and 11(a). It takes approximately 4 ms to reach a new battery current and active power references with the two methods. At the same time, the DC-link voltage v_{dc} can also be controlled to the desired value 200 V in both charging and discharging modes. However, from Fig. 10(b), it can be seen that the DC voltage has a small steady state error in the new working condition (discharging mode). The reason for this error is that the PI coefficients are selected for the charging operation. When the system requirements change, the PI coefficients are fixed, which is not the best set for the new condition. Compared with the conventional method, the DC voltage from the proposed method shows better performance with no steady state error in Fig. 11(b). In addition, the active power obtained from the proposed method presents less ripple compared with the conventional one during the charging operation. Since there is no reactive power transferred, the grid current i_a is in phase with the associated source voltage v_a in the charging mode and out of phase with v_a while discharging the power to the grid, as depicted in Figs. 10(d) and 11(d). The current from the proposed method also shows less distortion.

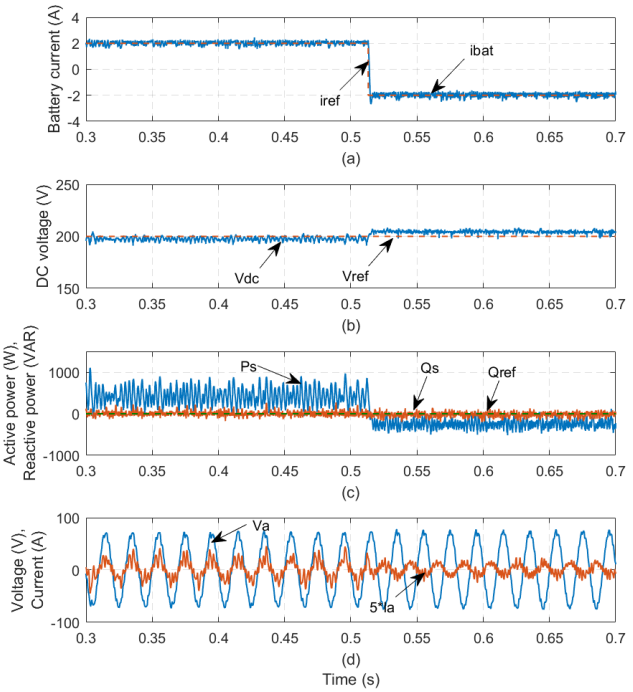

FIGURE 10. Conventional MPC: Step in the battery current reference i_{bat}^{ref}.

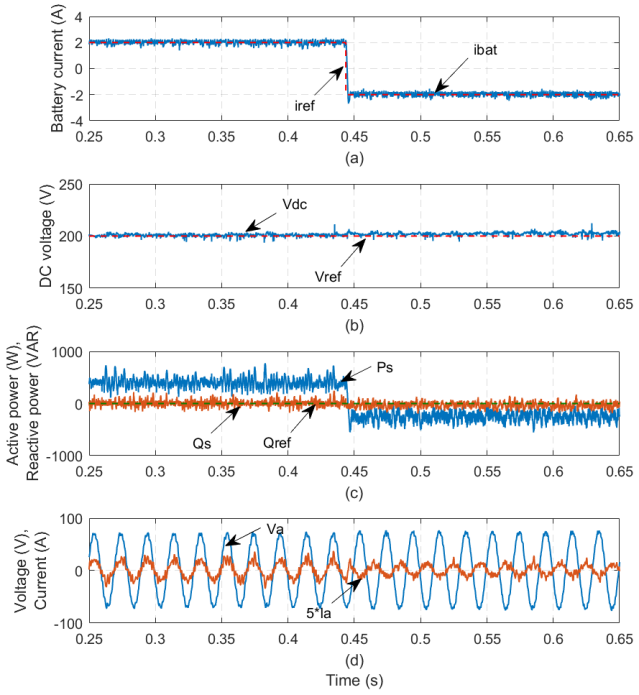

FIGURE 11. Proposed MPC: Step in the battery current reference i_{bat}^{ref}.

C. DC-LINK VOLTAGE TRACKING

Another objective of the proposed MPC is to track the DC-link voltage v_{dc}^{ref}. It is important to verify that the proposed controller can track the voltage reference while delivering the expected current in both charging and discharging operation. Figs. 12 and 13 show the performance obtained

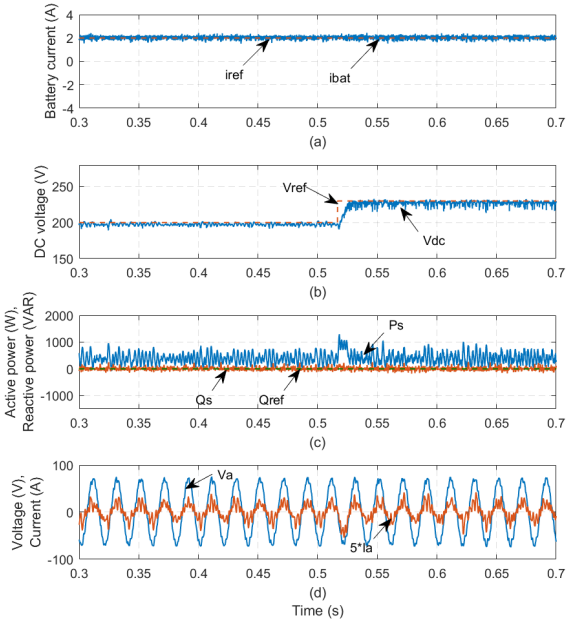

FIGURE 12. Conventional MPC: Step in the DC voltage reference v_{dc}^{ref} during charging operation.

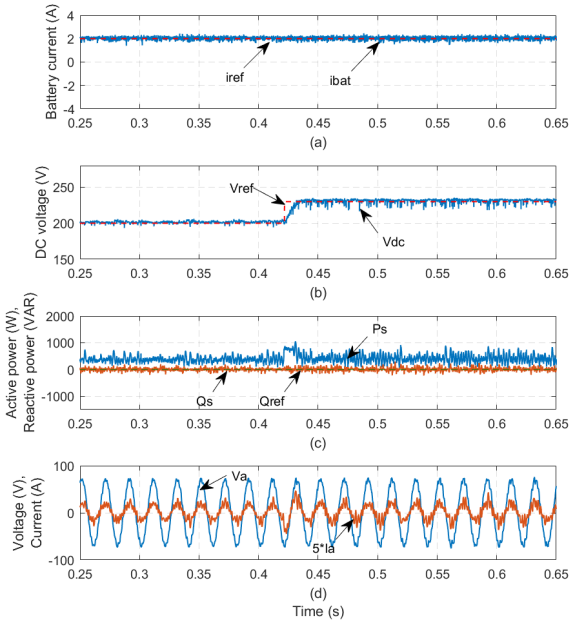

FIGURE 13. Proposed MPC: Step in the DC voltage reference v_{dc}^{ref} during charging operation.

from the conventional MPC scheme and the proposed method when charging the power to the EV battery, respectively. From Figs. 12(a) and 13(a), it can be seen that the current keeps at 2 A to charge the EV battery using both methods. The initial DC voltage is set to be $v_{dc}^{ref} = 200$ V. Then an increasing step is applied on this voltage reference as $v_{dc}^{ref} = 230$ V at time instant $t = 0.52$ s and 0.42 s in both schemes, respectively. It takes around 15 ms response time to reach the new DC voltage demand in both methods. Both control schemes present a good tracking performance in DC voltage with no overshoot/undershoot. To protect the system components, the source current is limited to $I_{max} = 7$ A, which results in a maximum active power P_{max} (around 750 W) in the proposed method. In the conventional method, a saturation block is applied to guarantee the generated active power reference from the PI controller within the above range (750 W). It can be noticed in Figs. 12(c) and 13(c) that the reactive power is still controlled to 0 VAR for a unity power factor operation. Therefore, the grid current is in phase with its associated voltage all the time. Similarly, the grid current in the proposed method shows a better performance than the conventional one.

Figs. 14 and 15 show the performance obtained from the conventional and proposed methods during the discharging mode where the active power is delivered from the load to the grid. Similar results are achieved by both control methods. The first target, the battery current, is controlled to the expected value (-2 A). Same as the performance in the charging operation, the response time is around 15 ms for the DC voltage and active power reaching the new demand for two method. Compared with the conventional method with a small overshoot around 3 V in the DC voltage, the proposed

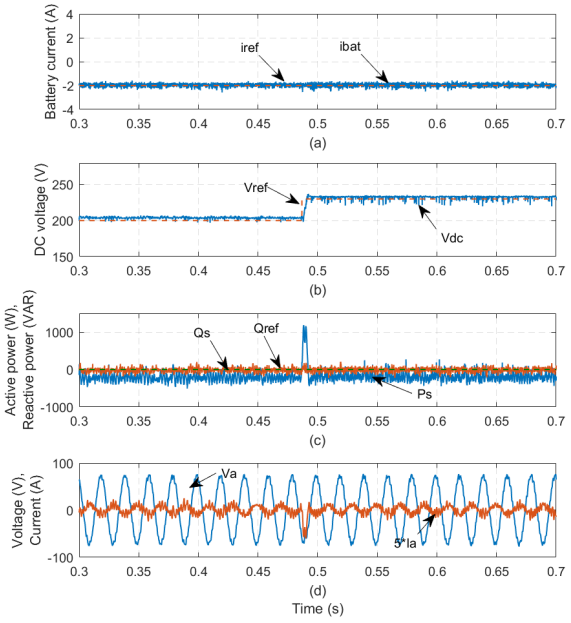

FIGURE 14. Conventional MPC: Step in the DC voltage reference v_{dc}^{ref} during discharging operation.

method can reach the new demand without any overshoot, as depicted in Figs. 14(b) and 15(b). Since the active power is transferred from the EV to the load and no reactive power is delivered, the grid current is out of phase with its associated voltage, as shown in Figs. 14(d) and 15(d).

D. REACTIVE POWER TRACKING

Besides tracking the battery current, DC voltage and active power, another main use for this bidirectional EV charger is

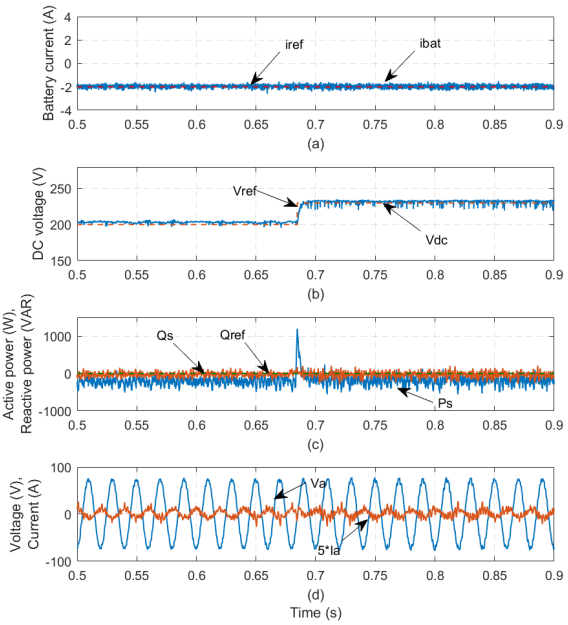

FIGURE 15. Proposed MPC: Step in the DC voltage reference v_{dc}^{ref} during discharging operation.

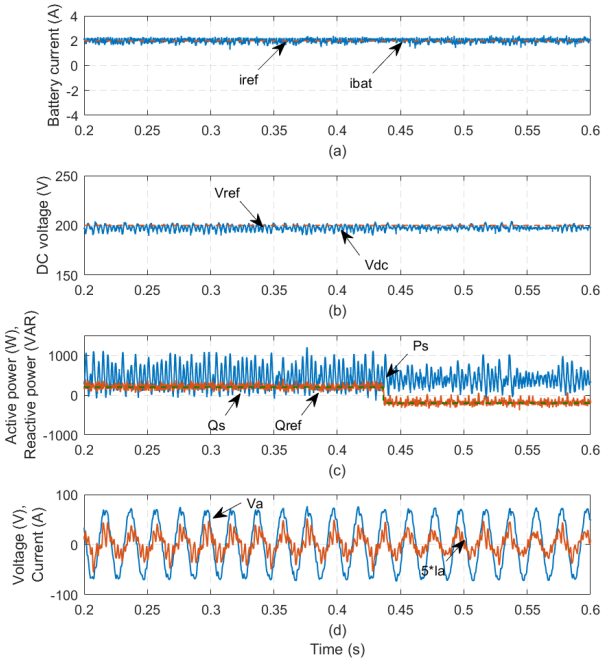

FIGURE 16. Conventional MPC: Step in the reactive power reference Q_s^{ref} during charging operation.

to compensate the reactive power for the main power grid, functioning as a static VAR compensator. Therefore, it is important to verify if the proposed method can track the reactive power demand when maintaining the DC voltage and battery current, or the system can be controlled to different power factors as required. Figs. 16 and 17 illustrate the performance for the two methods with the reactive power step during the charging operation. The initial condition of the system considers a DC voltage $v_{dc}^{ref} = 200$ V, a charging current $i_{bat}^{ref} = 2$ A and a positive active power $P_s^{ref} = 300$ W. A initial reactive power $Q_s^{ref} = 200$ VAR is provided from the grid to the load, leading to a power factor of 0.832. As observe from the figures, the grid current lags its associated voltage by 33.7° in both methods. The active power and grid current obtained by the MPC with dynamic reference method show better performances than those by the traditional scheme, which has less ripple and distortion.

A decreasing step is applied in the reactive power reference Q_s^{ref} from 200 VAR to -200 VAR at time instant $t = 0.44$ s in the conventional method and $t = 0.66$ s in the proposed method, respectively. It can be seen that using the two methods the system can track the new reactive power reference quickly without affecting the battery current, active power, and DC voltage. The grid current leads its associated voltage 33.7° in the new condition.

Similar operation conditions are performed during the discharging mode in Figs. 18 and 19. EV battery functions as an active power generator to compensate the grid during the peak hours. The battery current is set to be -2 A delivering around 300 W power to the grid. With the initial reactive power 200 VAR and active power -300 W, the grid current lags its associated voltage by 123.7°. At approximately

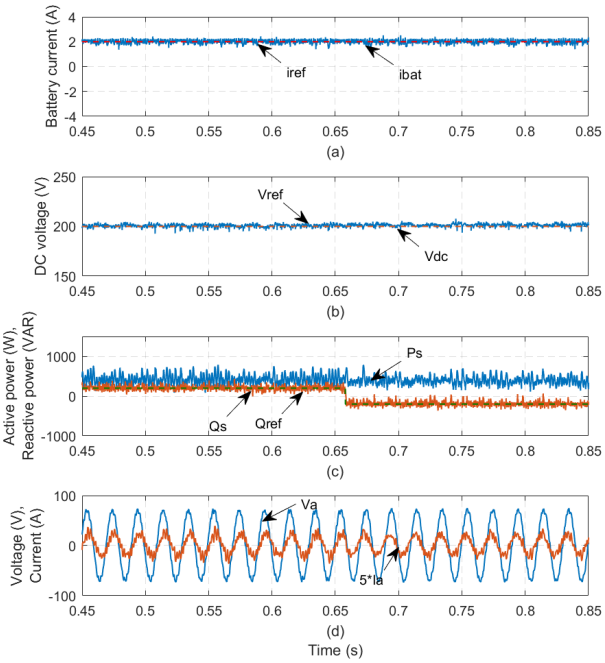

FIGURE 17. Proposed MPC: Step in the reactive power reference Q_s^{ref} during charging operation.

$t = 0.44$ s and 0.42 s in two methods, respectively, a step-down change in reactive power reference is introduced, from $Q_s^{ref} = 200$ VAR to $Q_s^{ref} = -200$ VAR. From Figs. 18(d) and 19(d), it can be seen that the source current i_a leads its phase voltage by 123.7° in the new steady state. Both methods can maintain the other objectives, such as the DC voltage, active power and the discharging current, to their

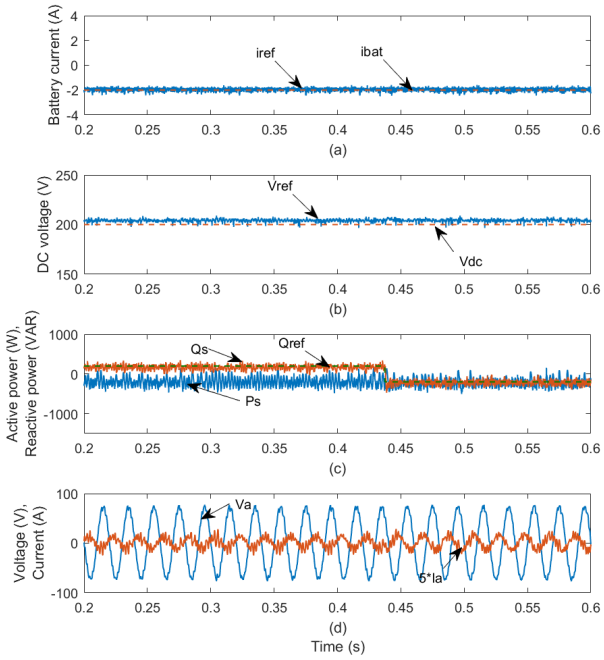

FIGURE 18. Conventional MPC: Step in the reactive power reference Q_s^{ref} during discharging operation.

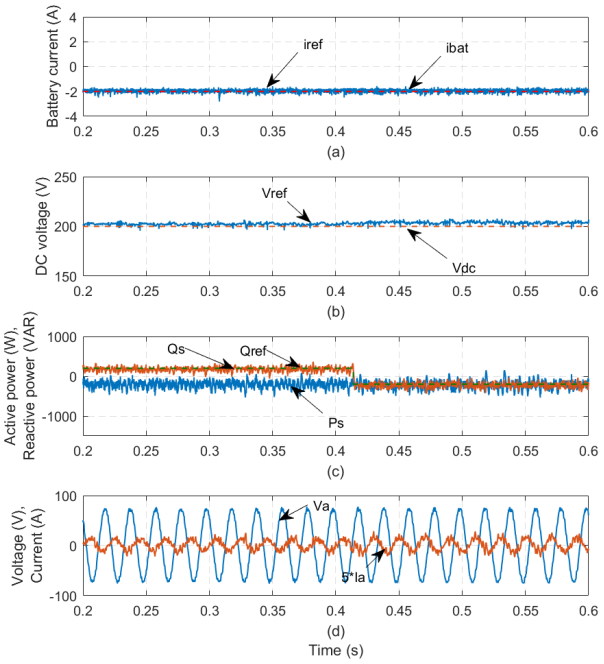

FIGURE 19. Proposed MPC: Step in the reactive power reference Q_s^{ref} during discharging operation.

original values. Better active power and grid current performance are achieved by the proposed method. This result is the same as the previous experimental results.

From the experimental results, it can be seen that the experimental grid current waveforms are noisy. The reason for this noisiness is due to the low sampling frequency limited by the dSPACE, the distorted grid voltage and the electromagnetic interference (EMI) in the PCB board and affecting the measurement equipment. For fair comparison, both the conventional method and proposed scheme used the same sampling frequency and system set up. Therefore, the noisiness of waveforms can be found in both methods, but they do not affect the stability of the system operation as it can be seen in Fig. 14 for instance. From the simulation and experimental results, the proposed method can have better performance, such as fast response and no overshoot.

VI. CONCLUSION

In this paper, a MPC method with dynamic reference for the bidirectional EV charger is proposed. In the conventional MPC method, a PI controller is used to track the DC voltage. However, it is hard to get a perfect set of coefficients by tuning based on different working conditions or system electric parameters. Therefore, a new method is proposed to providing a dynamic active power reference from the given DC voltage reference without any control loops. To make full use of the EV charger, the proposed method is capable of bidirectional power flow control in the charging and discharging operation modes. Since the EV charger can function as a static VAR generator, tracking the reactive power is another goal in this system. The proposed MPC can achieve muti-objective control of the battery current, DC voltage, active power and reactive power.

Numerous experimental results on a laboratory two-stage three-phase EV charger are compared and presented by using the conventional MPC and the proposed MPC with dynamic reference methods, respectively. Fast dynamic and good steady state performance are achieved for the above objectives during the charging and discharging modes in two methods. It is noted that no overshoot or undershoot of the DC voltage is introduced by using the proposed method. The DC voltage, reactive power and battery current can be controlled independently. The active power is associated with the battery current and the DC voltage references. With the proposed method, the active power has less ripple and the grid current has less distortion. No PI coefficients are needed to be tuned or selected by using the proposed method.

REFERENCES

[1] A. Dubey and S. Santoso, "Electric vehicle charging on residential distribution systems: Impacts and mitigations," *IEEE Access*, vol. 3, pp. 1871–1893, 2015.

[2] S. Y. Choi, B. W. Gu, S. Y. Jeong, and C. T. Rim, "Advances in wireless power transfer systems for roadway-powered electric vehicles," *IEEE J. Emerg. Sel. Topics Power Electron.*, vol. 3, no. 1, pp. 18–36, Mar. 2015.

[3] C. C. Mi, G. Buja, and S. Y. Choi, "Modern advances in wireless power transfer systems for roadway powered electric vehicles," *IEEE Trans. Ind. Electron.*, vol. 63, no. 10, pp. 6533–6546, Oct. 2016.

[4] Z. Tian, T. Jung, Y. Wang, F. Zhang, L. Tu, C. Xu, C. Tian, and X.-Y. Li, "Real-time charging station recommendation system for electric-vehicle taxis," *IEEE Trans. Intell. Transp. Syst.*, vol. 17, no. 11, pp. 3098–3109, Nov. 2016.

[5] M. Sjafie-Khah, E. heydarian-Forushani, and G. J. Osório, "Optimal behavior of electric vehicle parking lots as demand response aggregation agents," *IEEE Trans. Smart Grid*, vol. 7, no. 6, pp. 2654–2665, Nov. 2016.

[6] H. Farzin, M. Moeini-Aghtaie, and M. Fotuhi-Firuzabad, "Reliability studies of distribution systems integrated with electric vehicles under battery-exchange mode," *IEEE Trans. Power Del.*, vol. 31, no. 6, pp. 2473–2482, Dec. 2016.
[7] M. Kwon and S. Choi, "An electrolytic capacitorless bidirectional EV charger for V2G and V2H applications," *IEEE Trans. Power Electron.*, vol. 32, no. 9, pp. 6792–6799, Sep. 2017.
[8] Z. U. Zahid, Z. M. Dalala, and R. Chen, "Design of bidirectional DC/DC resonant converter for vehicle-to-grid (V2G) applications," *IEEE Trans. Transport. Electrific.*, vol. 1, no. 5, pp. 232–244, Oct. 2015.
[9] M. Yilmaz and P. T. Krein, "Review of the impact of vehicle-to-grid technologies on distribution systems and utility interfaces," *IEEE Trans. Power Electron.*, vol. 28, no. 12, pp. 5673–5689, Dec. 2013.
[10] E. L. Karfopoulos, K. A. Panourgias, and N. D. Hatziargyriou, "Distributed coordination of electric vehicles providing V2G regulation services," *IEEE Trans. Power Syst.*, vol. 31, no. 4, pp. 2834–2846, Jul. 2016.
[11] M. J. E. Alam, K. M. Muttaqi, and D. Sutanto, "Effective utilization of available PEV battery capacity for mitigation of solar PV impact and grid support with integrated V2G functionality," *IEEE Trans. Smart Grid*, vol. 7, no. 3, pp. 1562–1571, May 2016.
[12] M. C. Kisacikoglu, M. Kesler, and L. M. Tolbert, "Single-phase on-board bidirectional PEV charger for V2G reactive power operation," *IEEE Trans. Smart Grid*, vol. 6, no. 2, pp. 767–775, Mar. 2015.
[13] M. Kesler, M. C. Kisacikoglu, and L. M. Tolbert, "Vehicle-to-grid reactive power operation using plug-in electric vehicle bidirectional off-board charger," *IEEE Trans. Ind. Electron.*, vol. 61, no. 12, pp. 6778–6784, Dec. 2014.
[14] V. Monteiro, J. G. Pinto, and J. L. Afonso, "Operation modes for electric vehicle in smart grids and smart homes: Present and proposed modes," *IEEE Trans. Veh. Technol.*, vol. 65, no. 3, pp. 1007–1020, Mar. 2016.
[15] J. Dannehl, C. Wessels, and F. W. Fuchs, "Limitations of voltage-oriented PI current control of grid-connected PWM rectifiers with LCL filters," *IEEE Trans. Ind. Electron.*, vol. 56, no. 2, pp. 380–388, Feb. 2009.
[16] R. Kadri, J. P. Gaubert, and G. Champenois, "An improved maximum power point tracking for photovoltaic grid-connected inverter based on voltage-oriented control," *IEEE Trans. Ind. Electron.*, vol. 58, no. 1, pp. 66–75, Jan. 2011.
[17] Y. Zhang, J. Gao, and C. Qu, "Relationship between two direct power control methods for PWM rectifiers under unbalanced network," *IEEE Trans. Power Electron.*, vol. 32, no. 5, pp. 4084–4094, May 2017.
[18] J. K. Nama and A. K. Verma, "An efficient topology for electric vehicle battery charging," in *Proc. IEEE PES Asia–Pacific Power Energy Eng. Conf. (APPEEC)*, Nov. 2017, pp. 1–6.
[19] T. Noguchi, H. Tomiki, S. Kondo, and I. Takahashi, "Direct power control of PWM converter without power-source voltage sensors," *IEEE Trans. Ind. Appl.*, vol. 34, no. 3, pp. 473–479, May 1998.
[20] T. He, D. Lu, and L. Li, "Model-predictive sliding-mode control for three-phase AC/DC converters," *IEEE Trans. Power Electron.*, vol. 33, no. 10, pp. 8982–8993, Oct. 2108. doi: 10.1109/TPEL.2017.2783859.
[21] J. Rodriguez and P. Cortes, *Predictive Control of Power Converters and Electrical Drives*, 1st ed. West Sussex, U.K.: Wiley, 2012.
[22] Y. Zhang, X. Wu, and X. Yuan, "A simplified branch and bound approach for model predictive control of multilevel cascaded H-bridge STATCOM," *IEEE Trans. Ind. Electron.*, vol. 64, no. 10, pp. 7634–7644, Oct. 2017.
[23] X. Li, H. Zhang, M. B. Shadmand, and R. S. Balog, "Model predictive control of a voltage-source inverter with seamless transition between islanded and grid-connected operations," *IEEE Trans. Ind. Electron.*, vol. 64, no. 10, pp. 7906–7918, Oct. 2017.
[24] W. Song, Z. Deng, S. Wang, and X. Feng, "A simple model predictive power control strategy for single-phase PWM converters with modulation function optimization," *IEEE Trans. Power Electron.*, vol. 31, no. 7, pp. 5279–5289, Jul. 2016.
[25] Y. Zhang, Y. Peng, and H. Yang, "Performance improvement of two-vectors-based model predictive control of PWM rectifier," *IEEE Trans. Power Electron.*, vol. 31, no. 8, pp. 6016–6030, Aug. 2016.
[26] S. Vazquez, J. Rodriguez, M. Rivera, L. G. Franquelo, and M. Norambuena, "Model predictive control for power converters and drives: Advances and trends," *IEEE Trans. Ind. Electron.*, vol. 64, no. 2, pp. 935–947, Feb. 2017.
[27] P. Cortés, J. Rodríguez, P. Antoniewicz, and M. Kazmierkowski, "Direct power control of an AFE using predictive control," *IEEE Trans. Power Electron.*, vol. 23, no. 5, pp. 2516–2523, Sep. 2008.
[28] Y. Xu and F. Li, "Adaptive PI control of STATCOM for voltage regulation," *IEEE Trans. Power Del.*, vol. 29, no. 3, pp. 1002–1011, Jun. 2014.
[29] M. Lasheen, A. K. A. Rahman, and M. Abdel-Salam, "Adaptive reference voltage-based MPPT technique for PV applications," *IET Renew. Power Gener.*, vol. 11, no. 5, pp. 715–722, Mar. 2017.
[30] S. Dusmez and A. Khaligh, "A compact and integrated multifunctional power electronic interface for plug-in electric vehicles," *IEEE Trans. Power Electron.*, vol. 28, no. 12, pp. 5690–5701, Dec. 2013.
[31] U. Yilmaz, O. Turksoy, and A. Teke, "Intelligent control of high energy efficient two-stage battery charger topology for electric vehicles," *Energy*, vol. 186, pp. 1–11, Nov. 2019.
[32] V. Monteiro, T. J. C. Sousa, and R. Leite, "Comprehensive analysis and experimental validation of five-level converters for EV battery chargers framed in smart grids," in *Proc. Int. Young Eng. Forum (YEF-ECE)*, May 2019, pp. 14–19.
[33] D. E. Quevedo, R. P. Aguilera, M. A. Perez, P. Cortes, and R. Lizana, "Model predictive control of an AFE rectifier with dynamic references," *IEEE Trans. Power Electron.*, vol. 27, no. 7, pp. 3128–3136, Jul. 2012.
[34] M. P. Kazmierkowski, F. Blaabjerg, and R. Krishnan, *Control Power Electronics: Selected Problems*. Millbrae, CA, USA: Academic, 2002, pp. 117–121.

TINGTING HE (S'14) received the B.E. and master's degrees in electrical engineering from Beijing Jiaotong University, Beijing, China, in 2012 and 2014, respectively, and the Ph.D. degree in electrical engineering from the University of Technology Sydney (UTS), Sydney, Australia, in 2018, where she was a Casual Academic with the Faculty of Engineering and IT, from 2015 to 2018. She is currently a Postdoctoral Fellow with Beijing Jiaotong University, Beijing. Her research interests include power electronics, electric vehicles, and predictive control.

MINGLI WU received the B.Sc. and M.Sc. degrees in electrical engineering from Southwest Jiaotong University, Chengdu, China, in 1993 and 1996, respectively, and the Ph.D. degree in electrical engineering from Beijing Jiaotong University (BJTU), Beijing, China, in 2006, where he has been a Professor with the School of Electrical Engineering, since 2008.

He is currently the Head of the School for the School of Electrical Engineering, Beijing Jiaotong University. His research interests include power supply for electric railways, digital simulation of power systems, and electric power.

DYLAN DAH-CHUAN LU (M'04–SM'09) received the B.E. and Ph.D. degrees in electronic and information engineering from The Hong Kong Polytechnic University, Hong Kong, in 1999 and 2004, respectively.

In 2003, he joined PowerELab Ltd., as a Senior Design Engineer, and was responsible for industrial switching power supply projects. From 2006 to 2016, he was a full-time Faculty Member with The University of Sydney, where he currently holds an honorary position. Since July 2016, he has been an Associate Professor with the School of Electrical and Data Engineering, University of Technology Sydney, Australia. His current research interests include efficient and reliable power conversion for renewable sources, energy storage systems, and microgrids.

Dr. Lu is a member of the Engineers Australia. He was a recipient of the Best Paper Award in the category of Emerging Power Electronic Technique from the IEEE PEDS 2015. He currently serves as an Associate Editor of the IEEE TRANSACTIONS ON CIRCUITS AND SYSTEMS II and the *IET Renewable Power Generation*.

RICARDO P. AGUILERA (S'01–M'12) received the M.Sc. degree in electronics engineering from the Universidad Tecnica Federico Santa Maria, Chile, and the Ph.D. degree in electrical engineering from the University of Newcastle (UN), Australia, in 2007 and 2012, respectively, where he was a Research Academician with the Centre for Complex Dynamic Systems and Control, from 2012 to 2013.

From 2014 to 2016, he was a Senior Research Associate with the Australian Energy Research Institute, University of New South Wales, Australia. Since 2016, he has been with the University of Technology Sydney, Sydney, Australia, where he is currently a Lecturer. His research interests include power electronics and theoretical and practical aspects of model predictive control.

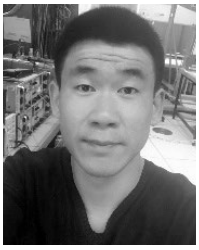

JIANWEI ZHANG received the bachelor's degree in electrical engineering from the Northwest A&F University, Yangling, China, in 2014, and the Ph.D. degree in electrical engineering from the University of Technology Sydney (UTS), Sydney, Australia, in 2018, where he was a Casual Academic with the Faculty of Engineering and IT, from 2015 to 2018. In 2018, he joined the Inner Mongolia University of Technology (IMUT), Hohhot, China, where he is currently an Associate Professor with the College of Electric Power. His research interests include control of power electronic converters, matrix converters, microgrids, and ac motor drives.

JIANGUO ZHU (S'93–M'96–SM'03) received the B.E. degree from the Jiangsu Institute of Technology, China, in 1982, the M.E. degree from the Shanghai University of Technology, China, in 1987, and the Ph.D. degree from the University of Technology Sydney (UTS), Australia, in 1995, all in electrical engineering.

He is currently the Head of the School for the School of Electrical and Information Engineering, The University of Sydney, Australia. His current research interests include electromagnetics, magnetic properties of materials, electrical machines and drives, power electronics, and green energy systems.